Electronic Supplementary Material (ESI) for Journal of Materials Chemistry A.

Electronic Supplementary Information

Unparalleled Mitigation of Membrane Degradation in Fuel Cells via a Counter-Intuitive Approach: Suppression of H_2O_2 Production at the Hydrogen Anode using a Pt_{skin}–PtCo Catalyst

Guoyu Shi,[a] Donald A. Tryk,[b] Toshio Iwataki,[b] Hiroshi Yano,[b] Makoto Uchida,[b] Akihiro Iiyama,[b] and Hiroyuki Uchida[a,b]*

[a]*Clean Energy Research Center, University of Yamanashi, Takeda 4, Kofu, 400-8510, Japan*
[b]*Fuel Cell Nanomaterials Center, University of Yamanashi, Takeda 4, Kofu, 400-8510, Japan*

*Corresponding author
E-mail: h-uchida@yamanashi.ac.jp; Fax: +81-55-220-8618; Tel: +81-55-220-8619

a) Catalysts used in the experiments

For the channel flow double electrode (CFDE) test, the catalyst employed was a PtCo alloy with a stabilized Pt-skin (Pt$_{xAL}$–PtCo: Pt$_{xAL}$ denotes a stabilized Pt skin with one to two atomic layer) supported on carbon black (specific surface area 780 m^2 g^{-1}) prepared in house by the nanocapsule method, followed by a deposition of Pt$_{xAL}$ (30 mass%-Pt loading).[1,2] A commercial Pt/C catalyst (c-Pt/C) (30 mass%-Pt loading, TEC10F30E) from Tanaka Kikinzoku Kogyo (TKK) was used for comparison. We also compared the results with those for two other catalysts, PtCo/C$_{HT}$ and a commercial c-Pt/CB (TEC10E50E, 50 mass%-Pt supported on carbon black with specific surface area 800 m^2 g^{-1}). The proprietary PtCo/C$_{HT}$ catalyst was designed and prepared as part of a collaboration with TKK by the nanocapsule method followed by a heat treatment (15 mass%-Pt loading) in order to closely mimic the characteristics of the in-house-prepared Pt$_{xAL}$–PtCo/C catalyst, but prepared with a more streamlined, scalable procedure. TEM images of these four catalysts are shown in Fig. S1 below. Based on EDX line scan analysis (Fig. S2), we have demonstrated for PtCo/C$_{HT}$, after potential cycling in 0.1 M HClO$_4$ at 80 °C, that a Pt skin with 1-2 atomic layers forms on the Pt-Co alloy surface, so that the PtCo/C$_{HT}$ is nearly identical with the in-house-prepared Pt$_{xAL}$–PtCo/C catalyst.

For the single cell test, the anode catalysts employed were PtCo/C$_{HT}$ and c-Pt/CB. As the cathode catalyst of the cell, a commercial Pt/GCB (Pt-loaded graphitized carbon black, 50 mass%-Pt loading, TEC10EA50E-HT) was used.

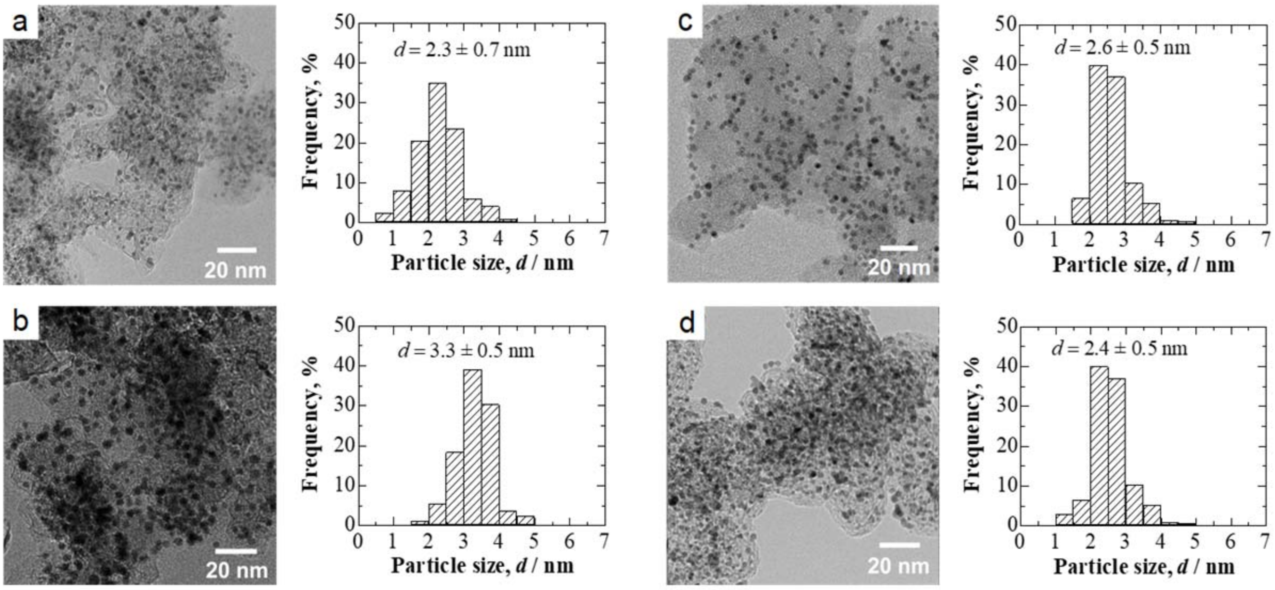

Fig. S1 TEM images and particle size distribution histograms of (a) c-Pt/C, (b) Pt$_{xAL}$–PtCo/C, (c) PtCo/C$_{HT}$, and (d) c-Pt/CB catalysts.

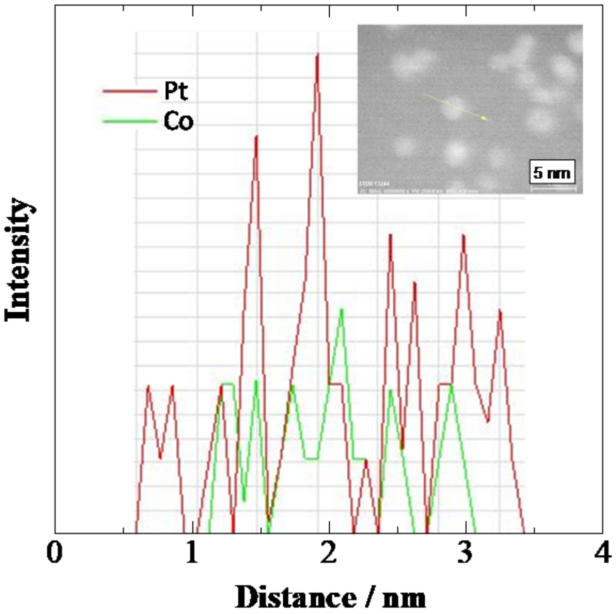

Fig. S2 Elemental distributions of Pt and Co obtained by STEM-EDX line scan analysis for a representative PtCo alloy nanoparticle of the PtCo/C_{HT} catalyst used in the single cell test.

b) CFDE measurements for H_2O_2 production rates in 0.1 M $HClO_4$ solution

The experiments were performed at 80 ºC based on the procedure as described earlier.[3] The working electrode (WE) was a glassy carbon (GC) substrate with a geometric area of 0.04 cm^2, on which Nafion-coated catalysts were uniformly dispersed. The use of the GC substrate was to minimize the H_2O_2 production. The catalyst amount loaded on GC was 8 μg_{Pt} cm^{-2}. The average thickness of Nafion film coated on the catalyst was 0.1 μm. A Pt wire was used as a counter electrode. All electrode potentials were referred to the reversible hydrogen electrode (RHE).

The electrolyte solution, 0.1 M $HClO_4$, was prepared from reagent grade chemicals and Milli-Q water (Millipore Japan Co., Ltd.). Polarization curves for the HOR were recorded under a flowing electrolyte solution (mean flow rate 111 cm s^{-1}) with positive potential scan. In order to evaluate the production rate of H_2O_2 on the catalysts during the HOR in the presence of O_2 (from air), we have developed a new method by the use of CFDE. First, the current density at the WE (j_W) for the HOR and the current density at a Pt collection electrode (CE, located at downstream of the WE) (j_C) were measured under a flow of H_2-purged solution. By changing the potential of the CE from 1.0 V to 1.4 V, we found that the j_C response to hydrogen oxidation was much decreased (80-95%), i.e., very small background current $j_C(H_2)$, due to passivation of the Pt surface. Moreover, the current was negligibly dependent on potential and thus changes in j_W for the HOR. The j_W and j_C values were measured under a flow of 10% air/H_2-saturated solution. The H_2O_2 formation current density $j(H_2O_2)$ was thereby calculated by use of the following equation:

$$j(H_2O_2) = [j_C(10\%\ \text{air}/H_2) - j_C(H_2)]/N \qquad (1)$$

where N is the collection efficiency of the CFDE ($N = 0.29$ herein). The potential dependent $j(H_2O_2)$ for all the catalysts are shown in Fig. S3.

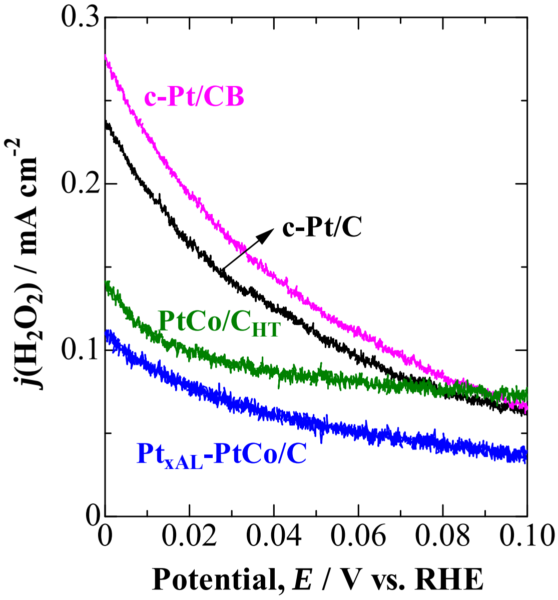

Fig. S3 Potential-dependent H_2O_2 oxidation current density, $j(H_2O_2)$, for c-Pt/C, Pt$_{xAL}$–PtCo/C, PtCo/C$_{HT}$, and c-Pt/CB measured in 10% air/H_2-saturated 0.1 M $HClO_4$ at 80 °C.

The kinetically-controlled current I_k for HOR at a given potential E was determined from the hydrodynamic voltammograms by use of the following equation:[4,5]

$$1/I = 1/I_k + 1/I_L \qquad (2)$$

where I is the observed current at a given potential and electrolyte (0.1 M $HClO_4$) flow rate, and I_L is the limiting current at the same flow rate. The kinetically-controlled mass activity, MA_k, at 20 mV vs. RHE for the HOR was determined by normalizing I_k to the Pt metal weight. The area-specific kinetic current densities j_k were obtained based on I_k and the electrochemically active area (ECA, see Table S1 below). The values of j_k and MA_k for all the catalysts are shown in Fig. S4.

Table S1 Electrochemically active areas (ECA) of Pt$_{xAL}$–PtCo/C, c-Pt/C, PtCo/C$_{HT}$, and c-Pt/CB measured at 80 °C in N_2-purged 0.1 M $HClO_4$ solution.

Catalyst	ECA / m^2 g^{-1}$_{Pt}$
Pt$_{xAL}$–PtCo/C	50.3
c-Pt/C	67.1
PtCo/C$_{HT}$	49.0
c-Pt/CB	70.9

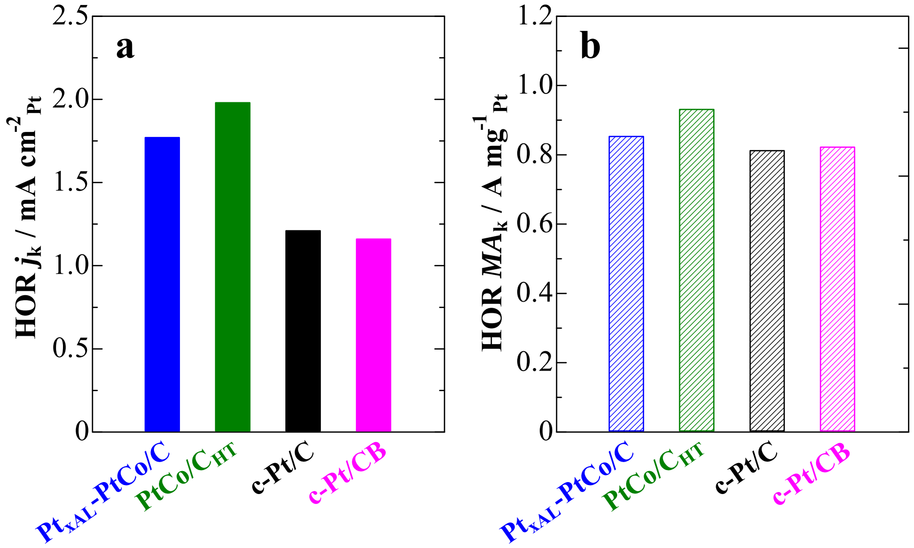

Fig. S4 HOR area-specific activity (a), j_k, and mass activity (b), MA_k, for Pt_{xAL}–PtCo/C, c-Pt/C, PtCo/C_{HT}, and c-Pt/CB measured in 10% air/H_2-saturated 0.1 M $HClO_4$ at 80 °C, calculated based on the kinetic current densities at 20 mV vs. RHE.

For comparison, conventional ORR measurements were conducted via the acquisition of hydrodynamic voltammograms at the working electrode in O_2-saturated 0.1 M $HClO_4$ at the same flow rate (111 cm s^{-1}) by scanning the potential from 1.0 to 0 V at 5 mV s^{-1}. Simultaneously, the current densities at the Pt collecting electrode (potential 1.4 V) for the oxidation of H_2O_2 were acquired. The H_2O_2 production current density $j(H_2O_2)$ was thus calculated as follows (with no need for background correction):

$$j(H_2O_2) = j_C(O_2)/N \tag{3}$$

As above, the value of N is 0.29. The ORR votammograms for Pt_{xAL}–PtCo/C and c-Pt/C are shown in Fig. S5, and the comparison of $j(H_2O_2)$ acquired by ORR and HOR experiments for all of the catalysts are shown in Fig. S6.

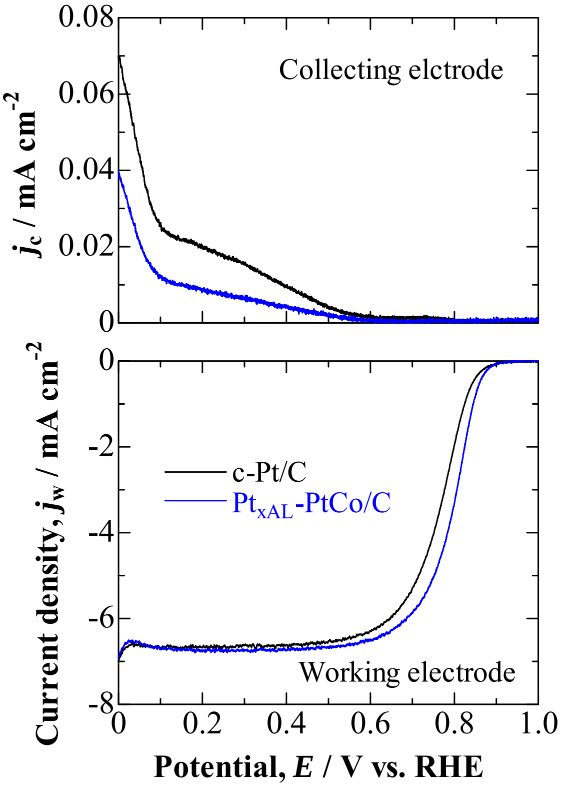

Fig. S5 Hydrodynamic voltammograms for the ORR in O_2-saturated 0.1 M $HClO_4$ at Nafion-coated Pt$_{xAL}$-PtCo/C and c-Pt/C electrodes at 80 °C. All data were obtained at a flow rate of 111 cm s^{-1} and a potential scan rate of 5 mV s^{-1}. The Pt collecting electrode was held at a potential of 1.4 V.

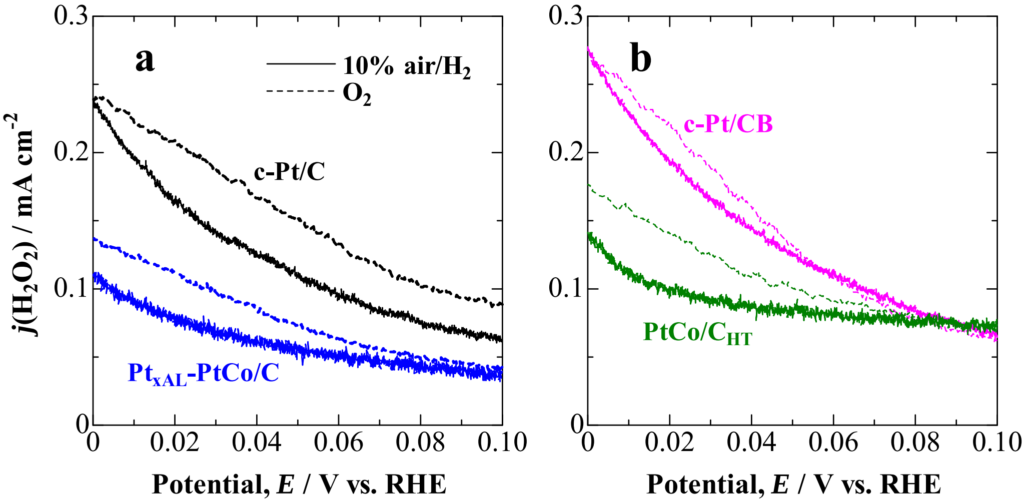

Fig. S6 Potential-dependent H_2O_2 oxidation current density, $j(H_2O_2)$, for (a) Pt$_{xAL}$-PtCo/C and c-Pt/C and (b) PtCo/C$_{HT}$ and c-Pt/CB measured in 10% air/H_2- and O_2-saturated 0.1 M $HClO_4$ at 80 °C.

c) DFT calculations

The density function theoretical (DFT) calculations were carried out by use of the DMol^3 package (BIOVIA, Materials Studio, Version 2019) with periodic boundary conditions.[6] Two different surfaces were modeled, a Pt(111)-3 × 3, 4-layer slab (Figs. S7 and S8) and, as in the previous work on the hydrogen evolution reaction (HER),[3] Pt(221) and Pt/Pt_3Co(221), 3-layer slabs, in which there are (110) steps and (111) terraces with three atomic rows width, with a 2 × 4 surface mesh (Figs. 3 and S9). The finest settings were used for the geometric optimization (convergence criteria, 1×10^{-5} Ha, maximum force 0.002 Ha/Å, maximum displacement 0.005 Å), which was carried out with density functional semicore pseudopotentials,[7] with a double-numeric quality basis set with polarization functions (dnp), and the final energies were calculated with all-electron scalar relativistic corrections. The gradient-corrected GGA functional used was developed by Perdew, Burke and Ernzerhof (pbe).[8] To facilitate scf convergence, kinetic energy was applied to the electrons (thermal smearing) of 0.005 Ha for Pt(111) and Pt(221) and 0.003 Ha for Pt/Pt_3Co(221).

For pure Pt(111) and Pt(221), the lattice parameter used for the face-centered cubic (fcc) structure was the standard experimental bulk value of 3.9239 Å. For Pt(221), the xyz coordinates of the 8 bottom-layer atoms were constrained to conform to those of the bulk structure, while the upper two layers were not constrained. For the Pt(111) model, the xyz coordinates of the 9 bottom-layer atoms were constrained to the bulk values, while the upper three layers were not constrained. For the Pt_{1AL}–PtCo(221) 2 × 4, 3-layer system, the model was based on bulk Pt_3Co, with a lattice parameter of 3.831 Å.[9] All of the Co atoms in the top layer were converted to Pt to simulate the Pt skin layer. The lower two layers were maintained as Pt_3Co, and the bottom-layer coordinates were constrained to bulk values.

For Pt(111), H_{UPD} and H_{OPD} were simulated in the "honeycomb" bridging arrangement, with an HUPD coverage θ_H of unity (9H), as described by Ishikawa and coworkers (Fig. S7).[10,11] O_2 was adsorbed in the end-on (Pauling) configuration (Fig. S7, left) at an atop site that can be occupied by H_{OPD}. To check the effect of the presence of H_{OPD}, the latter was added to the two remaining atop sites, with a θ_H of 11/9. The adsorption energies for H_{UPD} in Fig. S8, shown on the lower right axis, were calculated in the standard way by referencing to the energy of undissociated H_2:

$$\Delta E_{\text{2nH,ads}} = E_{\text{Pt slab-2nH}} - (E_{\text{Pt slab}} + nE_{\text{nH}_2}) \tag{3}$$

In order to calculate the adsorption energy of O_2 on the H-covered surfaces, the energy of the H-covered surface without O_2 was used as a reference, together with that of gas-phase O_2:

$$\Delta E_{\text{O}_2\text{, ads}} = E_{\text{Pt slab-O}_2\text{-nH}} - (E_{\text{Pt slab-nH}} + E_{\text{O}_2}) \tag{4}$$

The same equation was also used for the product in which O_2 had reacted with H to produce HO_2, as well as the transition state (Fig. S8).

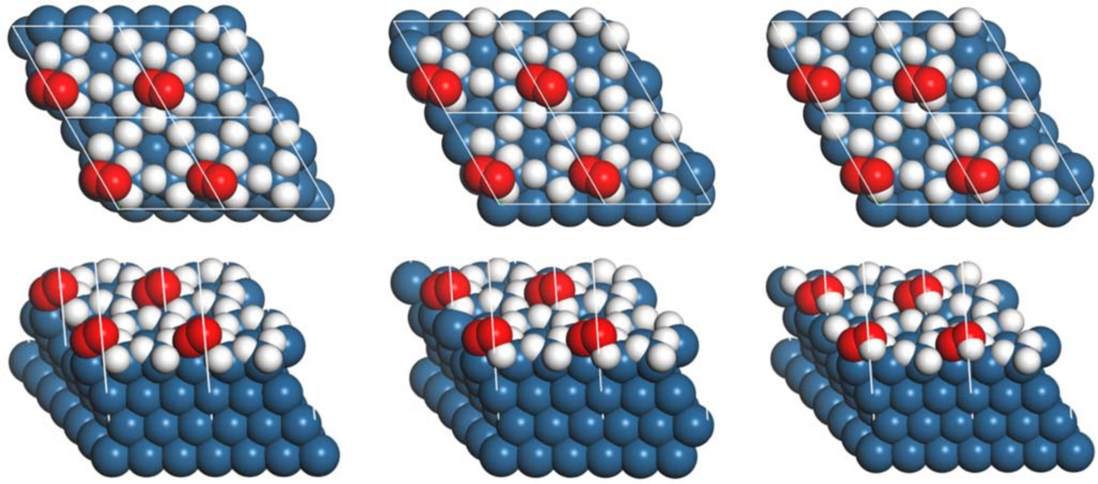

Fig. S7 Atomic models of the Pt(111)-3 × 3, 4-layer model with adsorbed O_2 and $9H_{UPD}$. The upper images are top views, showing four unit cells, and the lower images are merely tilted to show the reacting species more clearly. The initial state is at left, the transition state in the middle, and the product, with adsorbed HO_2 and $8H_{UPD}$ at the right. In the transition state, one of the bridging H_{UPD} converts to an atop H_{OPD}. Color scheme: Pt–dark blue; O–red; H–white.

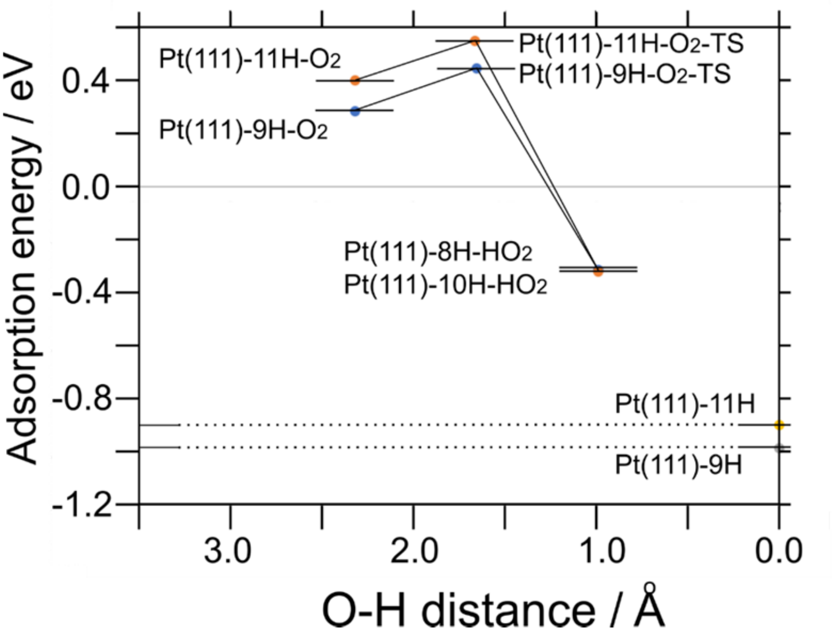

Fig. S8 DFT energy profiles calculated for the reaction $O_{2,ad} + 9H_{UPD,ad} \rightarrow HO_{2,ad} + 8H_{UPD,ad}$ on Pt(111) (lower profile) and $O_{2,ad} + 11H_{UPD,ad} \rightarrow HO_{2,ad} + 10H_{UPD,ad}$ (upper profile) surfaces, with the H-covered surfaces as reference, so the energies reflect the contribution of O_2 alone. The reaction coordinate is the O-H distance for the O-H bond in HO_2. The energies of the $9H_{UPD,ad}$ and $11H_{UPD,ad}$ systems can be seen at lower right, with the appropriate number of gas-phase H_2 molecules as reference.

For the Pt(221) and Pt/Pt_3Co(221) 2 × 4, 3-layer models with adsorbed O_2 + $2H_{UPD}$ + $1H_{OPD}$, the narrow (111) terraces were too narrow to accommodate a true honeycomb structure, so the 3H partial honeycomb was used, with the H_{OPD} situated on the lower terrace, close to the bridging O_2 adsorbed at the (110) step (Fig. S9). The models in Fig. S9 correspond to the energy vs. reaction coordinate presented in Fig. 3 in the main text. The calculated adsorption energies are shown in Table S2.

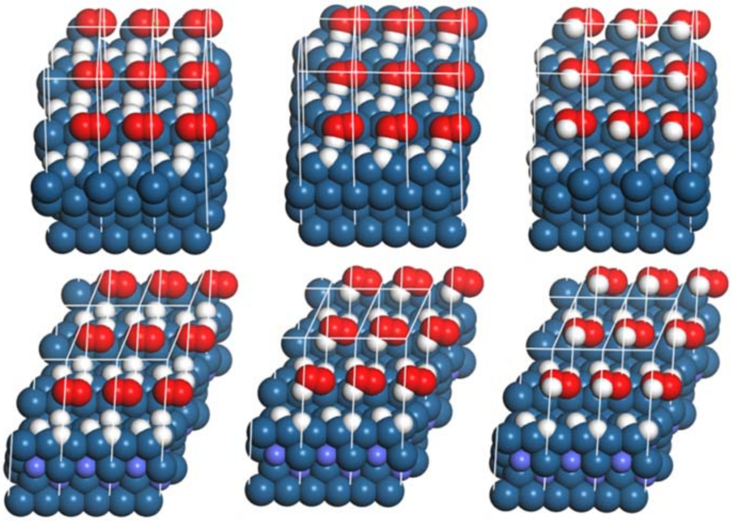

Fig. S9 Atomic models of the (upper) Pt(221) and (lower) Pt/Pt_3Co(221) 2 × 4, 3-layer models with adsorbed O_2 + $2H_{UPD}$ + $1H_{OPD}$, at left, which pass through the transition states in the middle to the product state HO_2 + $2H_{UPD}$ at right. These models correspond to the reaction profile shown in Fig. 3 in the main text. Each model shows a 3 × 3 array of unit cells. O_2 molecules are adsorbed in the bridging configuration along the (110) steps. Color scheme: Pt–dark blue; Co–light blue; O–red; H–white.

Table S2 Adsorption energies of O_2, O_2 + 3H, HO_2 + 2H, and 2H on Pt(221) and Pt/Pt_3Co(221) in eV.

Adsorbed species	Pt(221)	Pt/Pt_3Co(221)
O_2(br)/(110) step	−1.71	−1.22
O_2(br)/(110) step + $2H_{UPD}$ + H_{OPD} (111 terrace)	−1.71	−1.21
O_2(br) + $2H_{UPD}$ + H_{OPD} (transition state)	−1.43	−0.61
Activation energy	0.28	0.60
HO_2(br) + $2H_{UPD}$	−1.55	−1.42
$2H_{UPD}$ + H_{OPD} (111 terrace)	−0.99	−0.63
2H/(110) step (V-configuration)	−1.37	−0.96

Notes: the energies of O_2 + 3H, O_2 + 3H (transition state) and HO_2 + 2H are referred to the surface with 3H adsorbed ($2H_{UPD}$ + H_{OPD}). Comparing the O_2 adsorption energies with and without 3H, there is negligible effect of the presence of 3H. The H adsorption energies are referred to the appropriate number of gas-phase H_2 molecules (3/2 H_2 for 3H).

d) Preparation of membrane electrode assemblies (MEAs) and fuel cell OCV tests

Catalyst-coated membranes (CCMs) were prepared in the same manner as that described in the literature.[12] The catalyst pastes for the anode or cathode were prepared by mixing a catalyst, Nafion binder (IEC = 0.95-1.03 meq g^{-1}, D-521, Du Pont), ultrapure water, and ethanol by zirconia ball milling for 30 min. The mass ratio of Nafion binder to the carbon support (N/C) was adjusted to 0.70. These pastes were sprayed on both sides of a Nafion membrane (NRE 211, 25 μm thick, Du Pont) by use of a pulse-swirl-spray (PSS, Nordson) apparatus. The geometric electrode area was 29.2 cm^2, and the Pt loading amount of the catalyst layer was 0.50 ± 0.05 mg cm^{-2}. The CCMs were dried at 60°C for 12 h and hot pressed at 140 °C and 10 kgf cm^{-2} for 3 min. They were sandwiched between two gas diffusion layers (GDLs, 25BCH, SGL Carbon Group) and mounted into a spring-loaded Japan Automobile Research Institute (JARI) cell, which has serpentine flow channels in both the anode and the cathode graphite separators.

We compared the durability of Nafion membranes with two different anode catalysts and the identical cathode catalyst under accelerated operation conditions for fuel cell vehicles, i.e., a pressurized gas-open-circuit test. The cell temperature was maintained constant at 90 °C. Hydrogen (76% RH) and air (86% RH) were supplied to the anode and cathode, respectively and the flow rates were 200 mL min^{-1} for both gases. Due to the use of a large amount of Pt at the anode and cathode (0.5 mg_{Pt} cm^{-2}) for the accelerated stress test (AST) for the electrolyte membrane, the initial I-V curves of the cells with the two anode catalysts, c-Pt/CB and PtCo/C_{HT}, were nearly identical, as shown in Fig. S10. Then, the open-circuit voltage (OCV) of the cell at 160 kPaG was measured. At the initial point and every 200 h during the OCV test, hydrogen crossover from the anode to the cathode was measured by use of linear sweep voltammetry (LSV) with a potentiostat (PGST30 Autolab System, Eco-Chemie) at 90 °C and ambient pressure. Prior to the LSV measurement, hydrogen (100 mL min^{-1}) and nitrogen (150 mL min^{-1}) humidified at 76% RH, and 86% RH were supplied to the anode and cathode, respectively. The cell potential was swept from 0.15 to 1.0 V at a sweep rate of 0.5 mV s^{-1}. Then, in order to check changes in the ECA of the cathode and H_2 leak current, cyclic voltammograms (CVs) at the cathode were also measured under similar conditions to those for the LSV measurement, with the exception of the sweep rate being 20 mV s^{-1} from 0.08 to 1.0 V and the N_2 flow being stopped during the measurement. CVs measured every 200 h are shown in Fig. S11.

We measured the composition of nanoparticles of PtCo/C_{HT} in a pristine powder, in the catalyst layer of a reference CCM (untested), and that after the OCV test at 90 °C for 1000 h. The results are shown in Table S3. The Co content decreased from 45 ± 8 atom% (pristine catalyst) to 35 ± 11 atom% in the anode catalyst layer of an untested reference CCM. Such a decrease in Co content is ascribed to a partial dissolution of Co in the acidic catalyst ink (catalyst + Nafion binder solution) to form a Pt skin layer on the PtCo surface. After conditioning (potential cycling to measure the initial I-V curves) at 90 °C, an accelerated stress test (AST) of the PEM under open-circuit conditions in an H_2/air single cell was performed at 90 °C for 1000 h. By means of post-test analysis, the Co content was found to be 26 ± 8 atom%. The retention percentage of Co in the alloy was comparatively high, 74%, with a small standard deviation, even after 1000 h at 90 °C, demonstrating that the Pt skin layer was able to suppress the dealloying of Co.

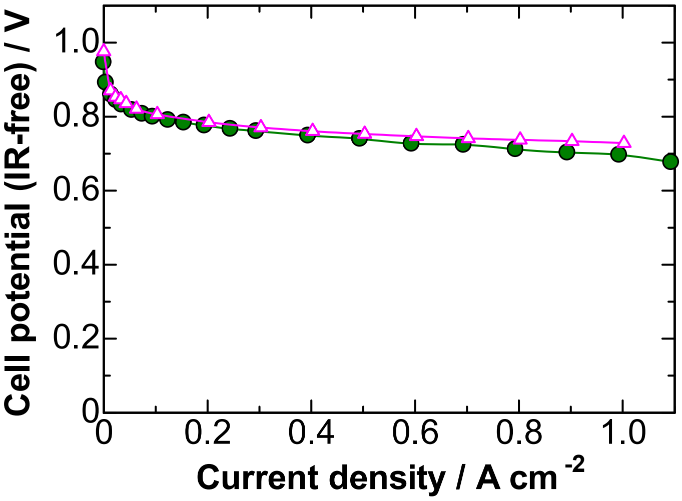

Fig. S10 Current-voltage (IR-free I-V) curves for single cells with two different anode catalysts (c-Pt/CB △ [12], PtCo/C_{HT} ●) and Pt/GCB cathode measured at 90 °C and ambient pressure. Hydrogen (76% RH) and air (86% RH) were supplied to the anode and cathode, respectively, and the flow rates were 200 mL min^{-1} for both gases.

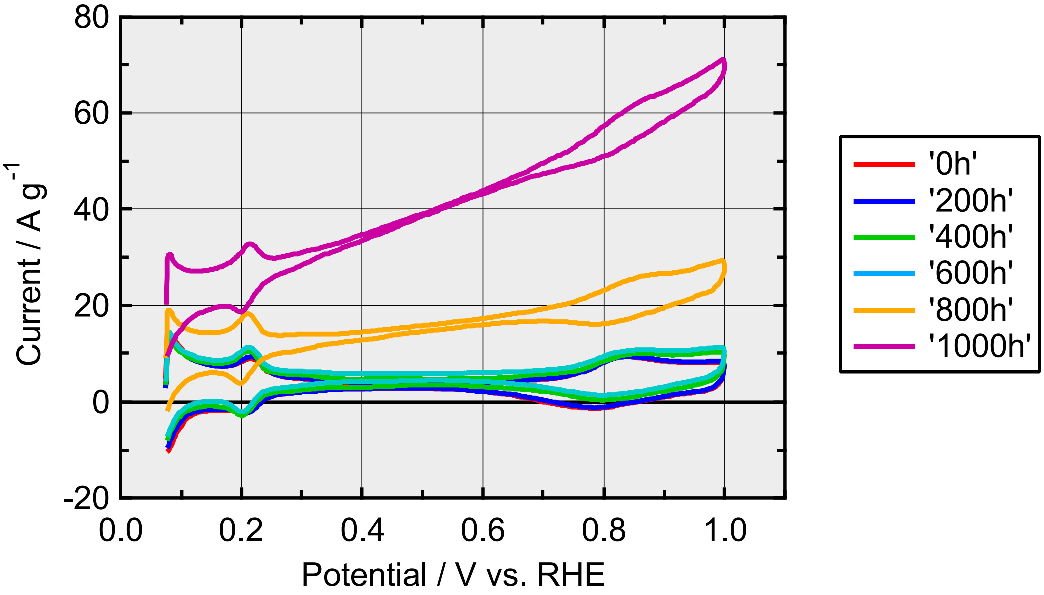

Fig. S11 Cyclic voltammograms (CVs) at a Pt/GCB cathode measured every 200 h of the OCV test at 90 °C and ambient pressure. Prior to the measurement, hydrogen (100 mL min^{-1}) and nitrogen (150 mL min^{-1}) humidified at 76% RH and 86% RH were supplied to the anode and cathode, respectively. The cell potential was swept from 0.08 to 1.0 V at a sweep rate of 20 mV s^{-1}. Nitrogen gas flow was stopped during the CV measurement.

Table S3 Changes in Co content (x in atom%) of nanoparticles for $Pt_{100-x}Co_x/C_{HT}$ pristine powder, in the catalyst layer of a reference CCM (untested), and that after the OCV test at 90 °C for 1000 h. The x values are averages, with standard deviations, of values for 10 individual $Pt_{100-x}Co_x$ nanoparticles analyzed using STEM-based EDX.

Catalyst	x, atom%
Pristine powder	45 ± 8
In the catalyst layer of a reference CCM (untested)	35 ± 11
In the catalyst layer of CCM after OCV test at 90 °C for 1000 h	26 ± 8

References

[1] M. Watanabe, H. Yano, D. A. Tryk and H. Uchida, *J. Electrochem. Soc.*, 2016, **163**, F455-F463.

[2] M. Chiwata, H. Yano, S. Ogawa, M. Watanabe, A. Iiyama and H. Uchida, *Electrochemistry*, 2016, **84**, 133-137.

[3] G. Shi, H. Yano, D. A. Tryk, S. Nohara and H. Uchida, *Phys. Chem. Chem. Phys.*, 2019, **21**, 2861-2865.

[4] H. Uchida, K. Izumi, K. Aoki and M. Watanabe, *Phys. Chem. Chem. Phys.*, 2009, **11**, 1771-1779.

[5] V. G. Levich, In *Physicochemical Hydrodynamics*; Prentice Hall: Englewood Cliffs, NJ, 1962; p. 112-116.

[6] B. Delley, *Int. J. Quant. Chem.*, 1998, **69**, 423-433.

[7] B. Delley, *Phys. Rev. B*, 2002, **66**, 155125-155133.

[8] J. P. Perdew, K. Burke and M. Ernzerhof, *Phys. Rev. Lett.*, 1996, **77**, 3865-3868.

[9] A. H. Geisler and D. L. Martin, *J. Appl. Phys.*, 1952, **23**, 375.

[10] Y. Ishikawa, J. J. Mateo, D. A. Tryk and C. R. Cabrera, *J. Electroanal. Chem.*, 2007, **607**, 37-46.

[11] J. J. Mateo, D. A. Tryk, C. R. Cabrera and Y. Ishikawa, *Mol. Simul.*, 2008, **34**, 1065-1072.

[12] R. Shimizu, J. Tsuji, N. Sato, J. Takano, S. Itami, M. Kusakabe, K. Miyatake, A. Iiyama and M. Uchida, *J. Power Sources*, 2017, **367**, 63-71.